Effect of Zn/Al Cation Ratio on Corrosion Inhibition Capabilities of Hydrotalcites Containing Benzoate Against Carbon Steel

Thu Thuy Pham[1], Anh Son Nguyen[1], Thu Thuy Thai[1], Gia Vu Pham[1], Ngoc Bach Ta[3], Thuy Duong Nguyen[1,†], and To Thi Xuan Hang[1,2,†]

[1]*Institute for Tropical Technology, Vietnam Academy of Science and Technology, 18 Hoang Quoc Viet, Cau Giay, Hanoi, Vietnam*
[2]*Graduate University of Science and Technology, Vietnam Academy of Science and Technology,*
18 Hoang Quoc Viet, Cau Giay, Hanoi, Vietnam
[3]*Institute of Materials Science, Vietnam Academy of Science and Technology, 18 Hoang Quoc Viet, Cau Giay, Hanoi, Vietnam*

Corrosion inhibitors based on Zn-Al hydrotalcites containing benzoate (ZnAlHB) with different molar ratios of Zn/Al were prepared with a co-precipitation process. Compositions and structures of the resulting hydrotalcites were studied with suitable spectroscopic methods such as inductively coupled plasma mass spectrometry (ICP-MS), ultraviolet-visible spectrophotometry (UV-Vis), scanning electron microscopy (SEM), X-ray diffraction (XRD), Fourier transform infrared spectroscopy (FTIR), and surface zeta potential measurements, respectively. Results of physico-chemical studies showed that crystallite sizes, compositions of products, and surface electrical properties were significantly changed when the molar ratio of Zn/Al was increased. The release of benzoate from hydrotalcites also differed slightly among samples. Anti-corrosion abilities of hydrotalcites intercalated with benzoate at a concentration of 3 g/L on carbon steel were analyzed using electrochemical impedance spectroscopy (EIS), polarization curve, energy-dispersive X-ray spectroscopy (EDX), and SEM. Corrosion inhibition abilities of benzoate modified hydrotalcites in 0.1 M NaCl showed an upward trend with increasing Zn/Al ratio. The reason for the dependence of corrosion resistance on the Zn/Al ratio was discussed, including changes in the microstructure of hydrotalcites such as crystal size, density, uniformity, and formation of ZnO.

Keywords: Corrosion, Hydrotalcites, Benzoate, Inhibitor

1. Introduction

Carbon steel and its alloys have been widely used in the structural, transportation industries and heavy industrial fields due to the advantage of cost-effectiveness, easy processing, strong mechanical strength and quality, and high mechanical properties [1-3]. Carbon steel is one of the most active metal materials, so it is very sensitive to corrosion in aqueous media at neutral and acidic pH. To protect carbon steel against corrosion, the addition in small quantities of corrosion inhibitor is an easy and high effective method [4,5].

Corrosion inhibitors can generally be classified into inorganic compounds and organic ones depending on their chemical composition [6,7]. Inorganic inhibitors (nitrites, chromates, dichromates and molybdates) can form a precipitated film on the metal surface which help prevent the corrosion metals, despite their advantages, some inhibitors were reported to caused environmental pollution

or present health risks [8,9]. Organic inhibitors containing N, O and S atoms can be absorbed on the metal surface by sharing the lone pair of electrons of heteroatoms to form a coordination bond that allows the material to adsorb onto a metal surface and separates metal from the aggressive solution [10,11]. However, these compounds often have complicated and low efficiency synthesis processes [12,13]. Therefore, the design next-generation of the corrosion inhibitor that can smartly protect where it has been corroded and provide sufficient long-term inhibitive performance have receiving a great deal of scientists in recent years [14,15]. Nanocontainers, such as metal organic frames [1,16], oxide nanoparticles [17] and hydrotalcites [18,19] with advantages like unique microporous structures, capability of controllable release of the adsorbent molecules into the media by exerting the adsorbent-surface interaction and without harming environment have been widely investigated [15].

Hydrotalcites (HTs), also known as layered double hydroxides (LDHs) or anionic clays, are well known as high anion-exchange substances due to their unique structure

†Corresponding author: ntd0801@gmail.com, ttxhang60@gmail.com

which consists of stacks of positively charged, mixed-metal hydroxide layers [20,21]. Therefore, by using hydrotalcites as corrosion inhibitors, they can release the inhibitive ions while absorbing chlorine anions. Recently, the research found that Zn-Al and Mg-Al HTs intercalated with inorganic inhibitors as molybdate [21-23], tungstate [24,25], vanadate [21,26] anions can effectively increase the corrosion resistance of magnesium alloys, because the interlayer anions were partially exchanged with chloride anions by ionic exchange and the invasive chloride ions were held by the hydrotalcite interlayer [22]. The Mg-Al HTs intercalated with 8-quinolinol (8HQ) showed the effective corrosion inhibition of 8HQ to Mg alloy due to the existence of chemisorption owing to formation of a complex chelate, (bis (8-hydroxyquinolinato) magnesium, $Mg(HQ)_2$), between 8HQ anions and dissolved Mg^{2+} [27].

Mg–Al and Zn–Al HTs [28,29] with vanadate or divanadate [30] anion showed promising results in active corrosion protection of aluminum alloys. The active corrosion protection of AA2024 by a bilayer system consisting of a hydrotalcite conversion layer coated by a sol-gel film was studied [31].

Wu et al. [32] developed the preparation of Zn-Al HTs intercalated with different inorganic inhibitor ions by ion exchange. The results showed that the HTs loaded with inhibitors could provide effective corrosion protection for carbon steel in the simulated concrete pore (SCP) solution. An incorporation of organic anions such as benzoate [32], sebacate [33] and 2-benzothiazolythio-succinic acid [33-36], into the interlayer space of hydrotalcite decreases significantly the corrosion rate of carbon steel.

Several researches show that size, charge and ratio of metal cations can affect charge and orientation of anions as well as relative amount of crystal water which determine crystal structure parameters of HTs, bond strength, anion exchange capacity and corrosion resistant capacity [37-39]. In our previous works, Zn-Al HTs intercalated with benzoate were prepared by co-precipitation method, incorporated in solvent free epoxy coatings and applied on carbon steel [33,40]. The results indicated that a long-term protection was obtained for carbon steel.

In present study, Zn-Al HTs containing benzoate (ZnAlHB) with the different molar ratio of Zn/Al were fabricated and studied on the effect of cation ratio on anticorrosion abilities on carbon steel. The structure, composition, chemical composition and morphology of the Zn-Al HTs containing benzoate (ZnAlHB) with the different molar ratio of Zn/Al were investigated by inductively coupled plasma mass spectrometry (ICP-MS), ultraviolet-visible spectrophotometry (UV-Vis), scanning electron microscopy (SEM), X-ray diffraction (XRD)

and Fourier transform infrared spectroscopy (FT-IR), the surface zeta potential measurements. Moreover, the effect of cation ratio on anticorrosion abilities was explored using electrochemical impedance spectroscopy (EIS), polarization curve, energy-dispersive X-ray spectroscopy (EDX), and SEM.

2. Experimental Methods

2.1. Materials and samples preparation

Aluminum nitrate nonahydrate ($Al(NO_3)_3.9H_2O$) (98%), Zinc nitrate hexahydrate ($Zn(NO_3)_2.6H_2O$) (98%) from Sigma Aldrich were used for fabrication of hydrotalcite. Sodium hydroxide (NaOH) (98%) from Sigma Aldrich and sodium benzoate ($C_7H_5O_2Na$) (99%) from VWR as an organic compound were used.

ZnAl hydrotalcite containing benzoate (ZnAlHB) was fabricated by the co-precipitation reaction with different ratio of Zn/Al = 2/1, 3/1, 4/1. Solution A is a salt mixture of $Zn(NO_3)_2$ and $Al(NO_3)_3$ (molar ratio of Zn^{2+}/Al^{3+} = 2/1, 3/1, 4/1). Solution B is a mixture of two solutions: benzoate solution and sodium hydroxide solution. Solution B was kept under nitrogen atmosphere at room temperature and pH = 8 – 9. Solution A was added to solution B with vigorous stirring. Then slurry was kept at 50 ℃ for 24 h under nitrogen atmosphere. The white precipitation formed was washed with large amounts of degassed distilled water before drying at a temperature of 70 ℃ for 24 h.

The used substrate in this work was carbon steel XC35 rod (1 cm^2 cross-section) having chemical composition was C = 0.35 wt%, Mn = 0.65 wt%, Si = 0.25 wt%, P = 0.035 wt%, S = 0.035 wt% and Fe = balance. To evaluate the inhibitive efficiency in 0.1 M NaCl solution, the used carbon steel rod was covered by a heat-shrinkable sheath (left only the tip of the cylinder in contact with the solution). The specimens were polished with SiC papers down to grade of 1200, washed with ethanol, and dried in warm air.

2.2. Analytical methods

Inductively coupled plasma mass spectrometry (ICP-MS) was used to determine the contents of Zn and Al in ZnAlHB hydrotalcites. The results were obtained on ICP-MS Agilent Technologies 7693.

UV-Vis spectroscopy was measured on GBC Cintra 40 spectrometer used to determine the content of benzoate in ZnAlHB and release of benzoate from ZnAlHB. The wavelength region was in the range of 200 – 400 nm. The samples were prepared at 3 g/L concentration in 0.1 M NaCl solution for release test.

The amount of benzoate in ZnAlHB was determined by the following protocol: 0.03 g of ZnAlHB was dissolved in

1.2 mL of 1 M HCl solution in 50-mL volumetric flask. Then distilled water was filled into the balance of volumetric flask. The absorbance of benzoate was monitored by UV–Vis spectrophotometer at λ_{max} = 225 nm. Based on the benzoate standard curve, the concentration of benzoate in the ZnAlHB was calculated. The standard curve was obtained from a series of benzoate standard solutions.

Powder X-ray diffraction patterns of ZnAlHB was obtained on Siemens diffractometer D5000 using CuKα radiation (λ = 0.15406 nm) at room temperature from 1° to 70° with scanning speed of 2.6°/min under air conditions.

Fourier transform infrared spectra of ZnAlHB powder was measured on Nexus 670 Nicolet spectrometer with resolution at 32 cm⁻¹ using the KBr method with transmission mode. The spectra were obtained in the region of 400 - 4000 cm⁻¹.

Field emission scanning electron microscope of ZnAlHB powder and coatings was operated on FESEM Hitachi S-4800 at a voltage of 5.0 kV.

The zeta potential measurements of the modified hydrotalcites in distilled water were carried out using a MALVERN Zetasizer Nano ZS. The concentrations of suspended solids were adjusted to 0.03 wt% before measurement.

Electrochemical measurements (EIS and potentiodynamic polarization) were carried out to study the corrosion performance of ZnAlHB in a 0.1 M NaCl solution using VSP 300 Bio-Logic. A classical three-electrode system was used, in which a XC35 rod with 1 cm² area as working electrode, a saturated calomel (SCE) and platinum electrode were used as reference and counter electrodes, respectively. The impedance diagrams were taken at the open circuit potential (OCP), under potentiostatic condition, over a frequency range from 100 kHz to 10 mHz with an amplitude of 5 mV. After 2 hours of exposure in 0.1 M NaCl solution containing ZnAlHB, the anodic and cathodic polarization curves were recorded at a scan rate of 1 mV s⁻¹. For each experiment, measurements were performed three times.

Steel surfaces after 2 h exposure to NaCl medium in absence and presence of ZnAlHB were analyzed by scanning electron microscopy/energy dispersive X-ray spectroscopy (SEM/EDX) on scanning electron microscope equipped (JSM-6510LV) with energy dispersive (INCAx-act, 51-ADD0085).

3. Results

3.1. Characterization of hydrotalcites containing benzoate

3.1.1. Element analysis and determination of inhibitor content

Elemental analysis data and inhibitor content for the synthesized hydrotalcites are presented in Table 1. The experimental atomic ratio of Zn/Al for ZnAlHB was determined by elemental analysis was 1.9/1, 2.9/1 and 3.6/1, respectively. These results close proposed ratio.

The loading amounts of benzoate in ZnAlHB were determined by UV-Vis. The concentration of benzoate (BZ) in the solution was determined by monitoring the absorbance at λ_{max} = 225 nm with UV–Vis spectroscopy. The calibration curve determined from a serie of standards BZ solutions [41]. The relationship between the absorbance and the BZ concentration was:

$$A = 8236\ C_{BZ} - 0.0121 \text{ with } R^2 = 0.999$$

where C is the concentration and A is the absorption intensity at λ_{max} = 225 nm.

The benzoate amounts in 2ZnAlHB, 3ZnAlHB, 4ZnAlHB were 26.8 wt%, 30.4 wt%, 27.5 wt%, respectively.

Formula of ZnAlHB HTs was given in Table 1. It was indicated that 2ZnAlHB still contained a small part of nitrat whereas the other hydrotalcites two have no nitrate in structure.

3.1.2. Fourier-Transform Infrared (FT-IR) Spectroscopy

Fig. 1 presents the FT-IR spectra of ZnAlHB HTs with different molar ratio of Zn/Al and the corresponding characteristic bands are given in Table 2. The broad absorption band at around 3450 cm⁻¹ and 1630 cm⁻¹ region assigned to OH group because of the presence of the surface water molecules and interlayer water molecules. There were medium absorption bands in the 400-700 cm⁻¹, which can be assigned to the lattice vibration of the metal (e.g. Zn-O, Al-O). The bands corresponding to of COO⁻ groups appeared as strong absorptions in the region around 1550 cm⁻¹ and 1400 cm⁻¹ [40]. From the FT-IR spectrum, it can be

Table 1. Elemental analysis data and chemical compositions of modified hydrotalcites

Samples	Content (wt%)			Atomic ratio Zn/Al	Atomic ratio Bz/Al	Formula
	Zn	Al	Bz			
2ZAHB	33.2	7.4	26.8	1.9	0.8	$Zn_{1.9}Al(OH)_{5.8}(NO_3)_{0.2}Bz_{0.8}.xH_2O$
3ZAHB	35.9	5.2	30.4	2.9	1.3	$Zn_{2.9}Al(OH)_{7.5}Bz_{1.3}.xH_2O$
4ZAHB	38.8	4.5	27.5	3.6	1.4	$Zn_{3.6}Al(OH)_{8.8}Bz_{1.4}.xH_2O$

Table 2. Characteristic bands of FT-IR spectra obtained for the ZnAlHB HTs with different molar ratio of Zn/Al

Group Samples	IR bands (cm^{-1})						
	OH^-	O-H	$CH_{aromatic\ ring}$	COO^-	NO_3	Al-O	Zn-O
2ZnAlHB	3443	-	1597	1552	1384	621	428
3ZnAlHB	3469	1633	1596	1551	1396	614	427
4ZnAlHB	3508	1632	1593	1533	1384	606	424
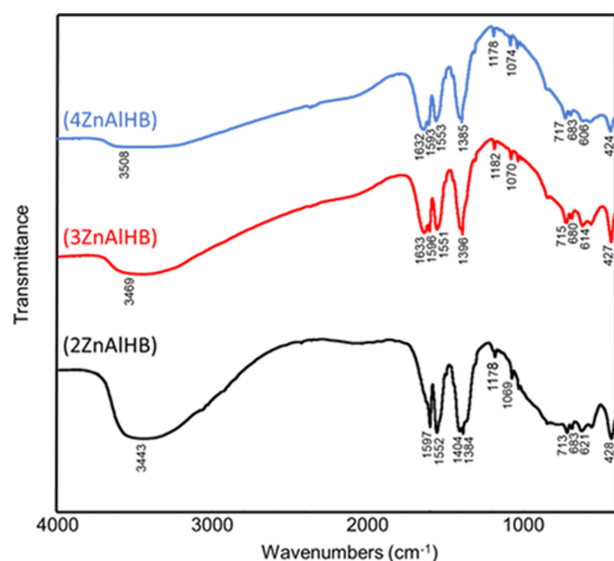
Fig. 1. FT-IR spectra of the ZnAlHB HTs with different molar ratio of Zn/Al

Fig. 2. Zeta potential of ZnAlHB HTs at 0.03 wt% concentration.

confirmed that the ZnAlHB HTs with different molar ratio of Zn/Al were successfully synthesized. However, in comparison with the FT-IR spectra of ZnAl-NO$_3$ HT, the characteristic band of asymmetric stretching vibration of the N-O in nitrate ions at around 1384 cm^{-1} was still observed, which was attributed to the appearance of an amount of nitrate anions in the products [40]. This spectral intensity is more clearly observed with the case of 2ZnAlHB in comparison with ones. These results are good agreement with obtained formula in above elemental analysis.

3.1.3. Zeta potential measurement

The surface charge properties of ZnAlHB HTs were estimated by zeta potential measurements in distilled water at 0.03 wt% as shown in Fig. 2. The zeta potentials of all ZnAlHB HTs are positive and higher than 30mV. The zeta potential of 2ZnAlHB is 40.8 mV and higher than the ones of other hydrotalcites (37.9 mV and 37.1 mV). The zeta potential reduced with an increase of Zn/Al ratio. These results can be explained that with a constant amount of aluminum, increase of the Zn/Al ratio corresponded to the
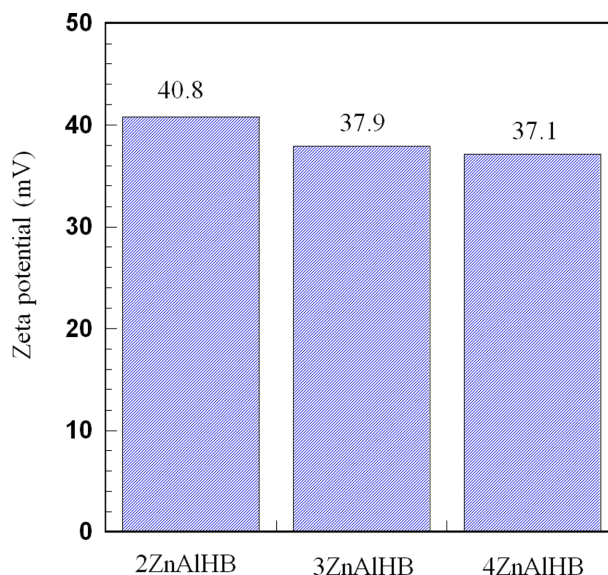
more Zn^{2+} density causing a decrease in the surface charge of the material.

3.1.4. XRD analysis

The XRD patterns of ZnAlHB HTs were presented in Fig. 3 and they exhibit distinguishable diffraction peaks observed at 2θ of 11.57°, 22.98°, 34.90°, 60.50° which corresponded to (003), (006), (012) and (110) planes as shown in Table 3 in the XRD standard of ZnAl hydrotalcite (JCPDS No. 38-0486) [40]. In comparison with ZnAl HTs [40], the XRD pattern of 2ZnAlHB, 3ZnAlHB and 4ZnAlHB shows the (003) reflection increasing to the basal spacing of 2.112 nm, 1.509 nm and 1.558 nm respectively. The increasing of d-spacing value between 2.11 and 1.51 nm confirms the intercalation of benzoate in the interlayer domain of hydrotalcite [40]. Therefore, the ZnAlHB HTs were obtained using the co-precipitation method.

The lattice parameters (a, c, u) and crystalline size of ZnAlHB HTs determined from XRD pattern are presented in Table 4. The lattice parameter a of hydrotalcite corresponds to the cation-cation distance within the brucite-like layer and is calculated by the equation a = 2 x d(110).

Table 3. XRD pattern of synthesized hydrotalcites

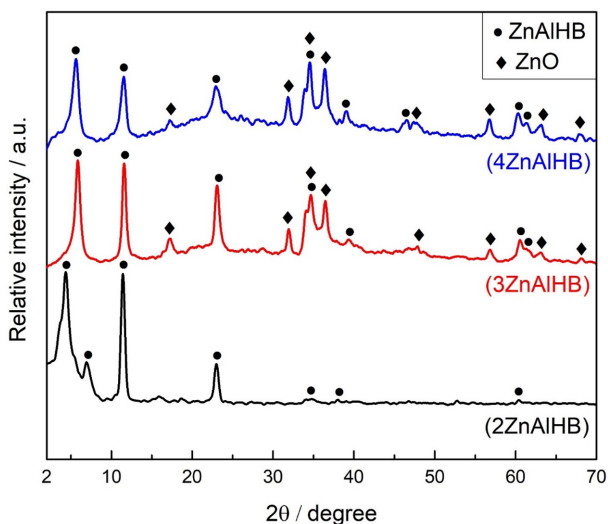| Hydrotalcite	(003)		(006)		(110)	
	2θ (°C)	d (nm)	2θ (°C)	d (nm)	2θ (°C)	d (nm)
2ZnAlHB	4.36	2.112	11.44	0.774	60.58	0.153
3ZnAlHB	5.86	1.509	11.58	0.763	60.32	0.153
4ZnAlHB	5.72	1.557	11.57	0.764	60.32	0.153

Fig. 3. XRD patterns of the ZnAlHB HTs with different molar ratio of Zn/Al

The lattice c parameter related to the thickness of the brucite-like layer and the interlayer distance is estimated by the equation c = 3 × d(003). The interlayer spacing u of brucite-like layers in HTs could be derived from d-spacing of 003 planes. The crystallite size of HTs can be obtained by using the Scherrer equation at the characteristic peak (006):

$$d = 0.9\lambda/FWHMcos\theta$$

where λ = 0.154 nm, FWHM, θ are the wavelength of X-rays, the full width at half maximum in radians and the diffraction angle for the peak (006), respectively.

The result showed that when Zn/Al molar ratio increased from 2ZnAlHB to 3ZnAlHB, the c parameter decreased from 6.069 nm to 4.527 nm and interlayer spacing u also reduced from 5.763 nm to 4.221nm. The higher value c of 2ZnAlHB can be explained by the interlayer interaction. Zn^{2+} density is more in higher Zn/Al ratio due to coulombic forces between anion and hydroxide may be changed. When Zn/Al molar ratio increased from 3ZnAlHB to 4ZnAlHB, the c parameter, as well as interlayer spacing u also gradually increased. That change could be explained by the substitution of small cations Al^{3+} (radius of 68 pm) by larger cations Zn^{2+} (radius of 83 pm) causing the expansion of HT unit cell, consequently, making the increase slightly in interlayer spacing u. The crystallite size of HTs were obtained by using the Scherrer equation at the characteristic peak (006). The crystallite size of HTs showed a downward trend when the molar ratio of Zn/Al increases. In addition, with changing molar ratio of Zn/Al, the composition of the product changes. While the XRD pattern of 2ZnAlHB was not any foreign peaks belonging to contaminations, for 3ZnAlHB and 4ZnAlHB samples, which appeared some new peaks attributable to ZnO (JCPDS No. 36-1451). This indicates that increasing concentration of zinc cation seemed to have significant effect on the presence of ZnO. Zinc oxide which was interweaved with the network of 3ZnAlHB and 4ZnAlHB crystals could work as a conditioner and could make the mutual orientation of benzoate ring planes in the interlayer space. Therefore, the increasing of interlayer spacing u from 3ZnAlHB to 4ZnAlHB completely depends on the change of molar ratio Zn/Al.

3.1.5. Scanning electronic microscopy

SEM images of ZnAlHB HTs are shown in Fig. 4. The

Table 4. Lattice parameters (c, a) and crystallite size of synthesized hydrotalcites

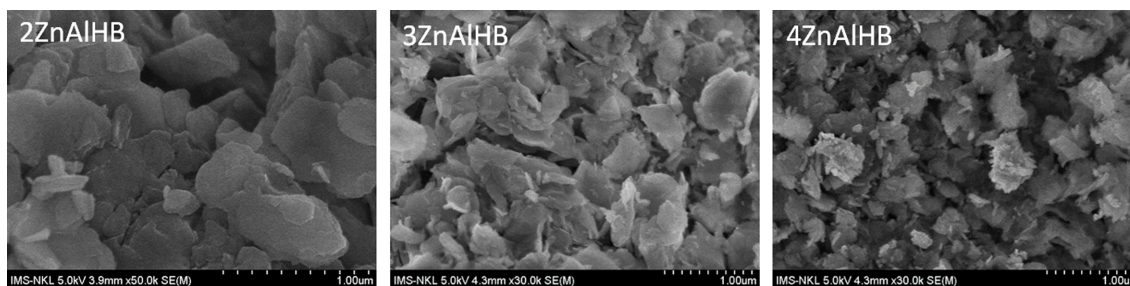| Hydrotalcite	Lattice parameter (nm)			Crystallite size (nm)
	a	c	u	
2ZnAlHB	0.306	6.069	5.763	23.212
3ZnAlHB	0.306	4.527	4.221	22.752
4ZnAlHB	0.306	4.671	4.365	11.030

Fig. 4. SEM images of ZnAlHB HTs

crystal size of ZnAlHB HTs tended to decrease slightly as the molar ratio of Zn/Al was increased from 2 to 4. All the samples show the typical plate-like morphology of hydrotalcite with particle sizes in the range from 200 nm to 500 nm. The morphologies of 3ZnAlHB and 4ZnAlHB are similar and are more separated than the one of 2ZnAlHB. 4ZnAlHB particles are smallest and most homogenous. This result is completely consistent to the result obtained by using the Scherrer's equation in XRD analysis. When Zn/Al molar ratio increased from 2ZnAlHB to 3ZnAlHB, the c parameter and crystallite size in the XRD analysis results decreased corresponding to the reduce in the thickness and size of the hydrotalcite sheet. That can be clearly observed in the SEM images, the HT sheets of 2ZnAlHB sample are thicker and larger than that of 3ZnAlHB sample. In the case of 4ZnAlHB sample, the c parameter and the crystallite size are lowest among samples and it has thinnest and smallest sheet.

3.2. Release of inhibitors from modified hydrotalcites

The corrosion process generally occurs in the presence of aggressive anions in the solution. The inhibitors release in the presence of anions is expected to impede corrosion and confer self-healing properties to the coatings. The influence of the Zn/Al ratio on the benzoate release from ZnAlHB HTs in 0.1 M NaCl solution at 3 g/L was also evaluated. The release of benzoate from 2ZnAlHB, 3ZnAlHB, 4ZnAlHB after different immersion times are shown in Fig. 5. It can be seen for all three solutions, there was a rapid release within the initial 120 minutes, followed by a slower release. The release of benzoate increased with growth of Zn/Al ratio. After 1440 minutes, the releases of benzoate from 4ZnAlHB, 3ZnAlHB, 2ZnAlHB were about 65%, 60% and 54%, respectively. The release of inhibitors from modified hydrotalcites is due to an exchange anion reaction which depends on the interaction between the intercalated anion and the positively charged hydroxide layer in hydrotalcites. The interlayer interactions in hydrotalcites are coulombic forces between the positively charged layers and the anions in the interlayer but also hydrogen bonding
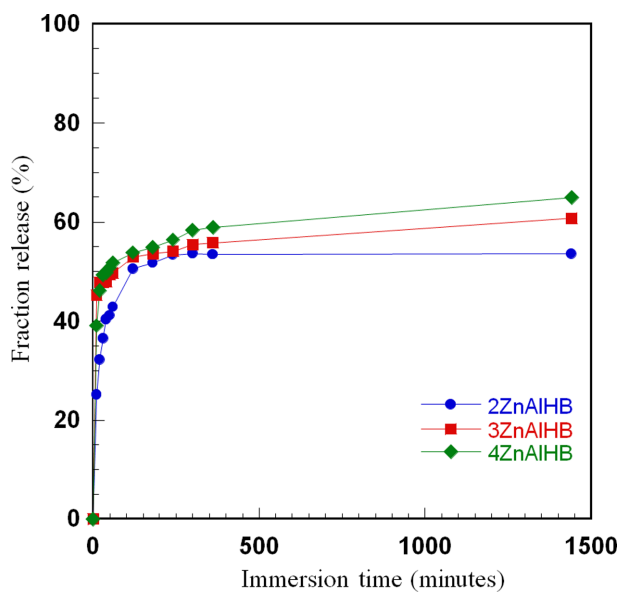

Fig. 5. Fraction released of ZnAlHB HTs in 0.1 M NaCl solution

between the hydroxyl groups of the layer with the anions and the water molecules in the interlayer [42,43]. The lower release of benzoate from hydrotalcites with lower Zn/Al ratio can be explained that with a constant amount of aluminum, reduction of the Zn/Al ratio corresponded to the less Zn^{2+} density causing an increase of the positively charged of layers or a stronger coulombic force. These obtained results seem to be consistent with those above analyses.

3.3. Corrosion inhibition effect of modified hydrotalcites

The polarization curves for the carbon steel electrode obtained after 2 h of immersion in 0.1 M NaCl solution without inhibitor and with ZnAlHB HTs at concentration of 3 g/L are presented in Fig. 6. The anodic curves are strongly modified by the presence of ZnAlHB HTs in comparison to the solution without inhibitors. It can be seen that the corrosion current density decreases significantly with the presence of ZnAlHB HTs and it was close for all ZnAlHB

THU THUY PHAM, ANH SON NGUYEN, THU THUY THAI, GIA VU PHAM, NGOC BACH TA, THUY DUONG NGUYEN, AND TO
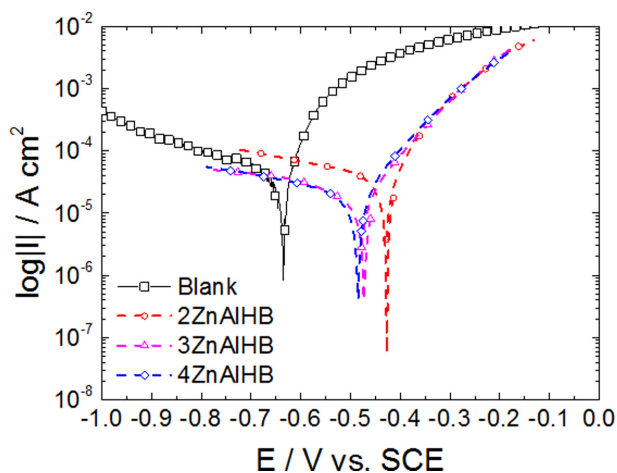THI XUAN HANG

Fig. 6. Polarization curves obtained for the carbon steel electrode after 2 h of immersion in 0.1 M NaCl solution without inhibitor and with different ZnAlHB HTs at 3 g/L
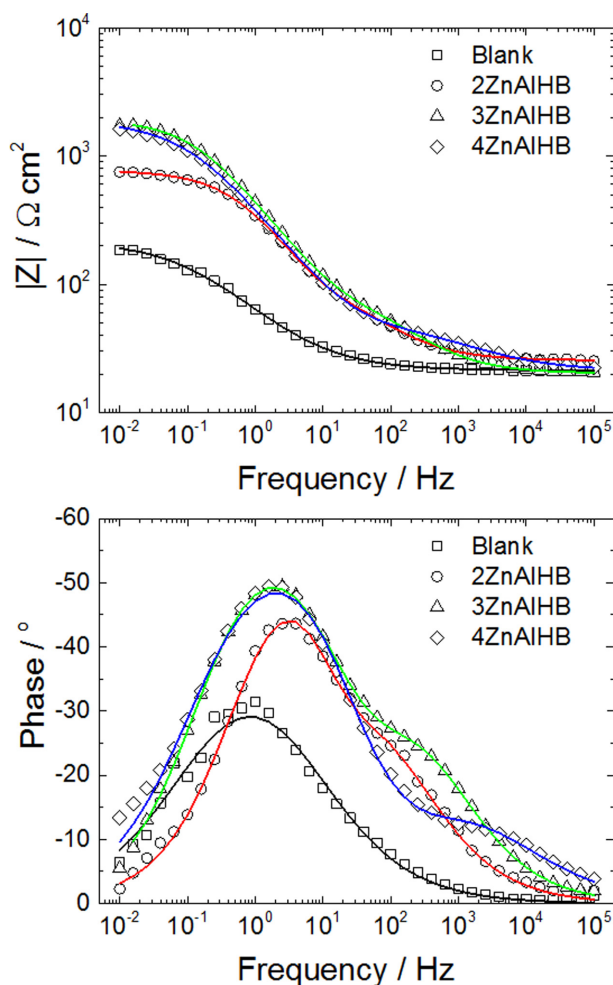

Fig. 7. Electrochemical impedance diagrams (Bode plots) obtained for the carbon steel electrode after 2 h of immersion in 0.1 M NaCl solution without inhibitor and with different ZnAlHB HTs at concentration of 3 g/L

HTs. The shift of the corrosion potential of all hydrotalcites towards more positive values (-0.43 V, -0.47 V and -0.48 V for 2ZnAlHB, 3ZnAlHB and 4ZnAlHB, respectively) than the one of blank sample (-0.63 V). These results showed that all ZnAlHB HTs are anodic inhibitors for carbon steel. The cathodic curve of 2ZnAlHB had a very slightly difference compared to the curve obtained in the blank solution. The cathodic curves measured in the solution containing 3ZnAlHB and 4ZnAlHB showed a decrease of cathodic current densities in comparison to the case of 2ZnAlHB. This different behavior among hydrotalcites samples can be explained the presence of ZnO in structure of 3ZnAlHB and 4ZnAlHB. So 3ZnAlHB and 4ZnAlHB can act as mixed inhibitor.

Fig. 7 shows impedance diagrams (Bode coordinates) obtained for the carbon steel in these solutions after 2 hours of immersion. For the solution containing ZnAlHB HTs, the impedance modulus and phase angle presented a difference compared to the curves obtained for the 0.1 M NaCl solution without inhibitors. The impedance module value increased with presence of ZnAlHB HTs and this value is higher with higher Zn/Al ratio.

Additionally, the inhibitor efficiency can be evaluated by using the value of the polarization resistance obtained from impedance diagram according to equation: $E\% = (R_p - R_{p0})/R_p$ [36]. In this equation, R_p and R_{p0} are the polarization resistances in the presence and the absence of inhibitor.

The measured values are reported in Table 5. It shows that the inhibitor efficiency of 3ZnAlHB (89.3%) and 4ZnAlHB (89.4%) is higher than that of 2ZnAlHB (77.3%). The higher inhibiting performance of ZnAlHB HTs having higher Zn/Al ratio compared to that of 2ZnAlHB HTs can be explained by inhibitor release abilities and the presence ZnO in hydrotalcite structure.

SEM photographs of steel surface were also taken after 2 h immersion in 0.1 M NaCl solution without and with ZnAlHB HTs at a concentration of 3 g/L and shown in Fig. 8. For steel surface immersed in 0.1 M NaCl solution without

Table 5. Polarization resistance and inhibition efficiency for carbon steel electrode after 2 h of immersion in the 0.1 M NaCl solution without inhibitor and with different ZnAlHB HTs at concentration of 3g/L

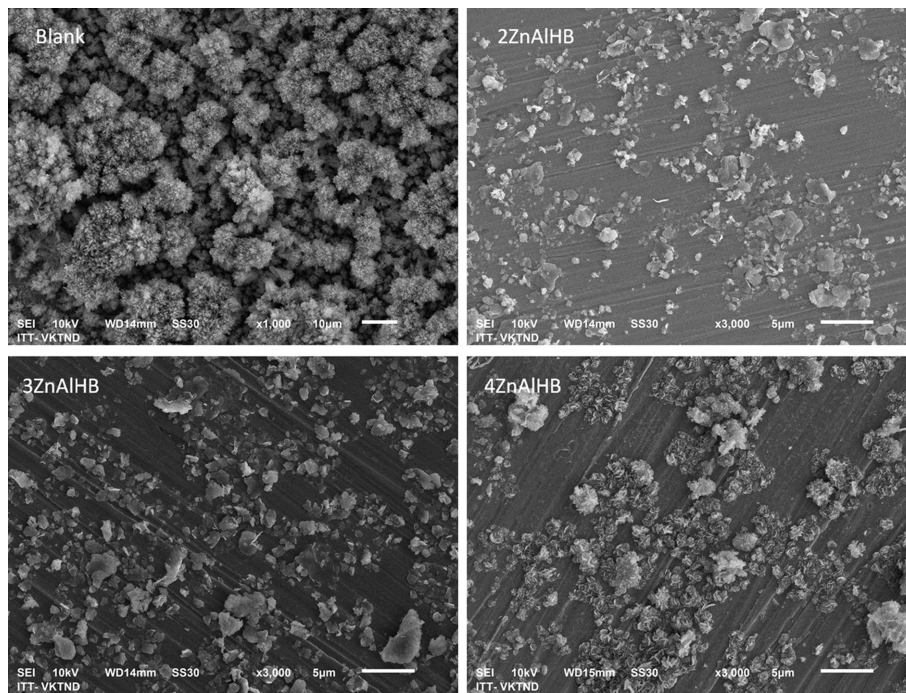| Sample	R_p ($\Omega.cm^2$)	Inhibition efficiency (%)
Blank	197	-
2ZnAlHB	867	77.3
3ZnAlHB	1840	89.3
4ZnAlHB	1867	89.4

Fig. 8. SEM photographs of steel surface after 2 h of immersion in 0.1 NaCl solution without inhibitor and with ZnAlHB HTs at a concentration of 3 g/L

Table 6. EDX elemental analysis of steel surface after 2 h immersion in 0.1 M NaCl solution without inhibitor and with hydrotalcites at a concentration of 3 g/L

Imersion medium	Zn (wt%)	Al (wt%)	O (wt%)	Fe (wt%)	C (wt%)
0.1 M NaCl	-	-	31.69	55.77	12.54
0.1 M NaCl + 2ZnAlHB	7.94	0.93	6.14	79.60	5.38
0.1 M NaCl + 3ZnAlHB	12.09	1.29	6.25	74.92	5.45
0.1 M NaCl + 4ZnAlHB	10.34	0.78	4.12	79.07	5.7

inhibitor, crystals of iron oxide are observed. In the case of 0.1 M NaCl solution containing ZnAlHB HTs, hydrotalcites can be detected on the steel surface but corrosion products are no more present. For solutions containing hydrotalcite with higher Zn/Al ratio, the hydrotalcite structures were more separated with smaller size in comparison with that of a solution with 2ZnAlHB. Finally, elemental analyses by EDX of the steel surface were also performed after 2 h immersion in 0.1 M NaCl solution without and with ZnAlHB HTs at a concentration of 3 g/L and presented in Table 6.

The EDX analysis shows a high oxygen content in the case without inhibitor. A lower oxygen content is revealed in the case of hydrotalcites loaded with benzoate. The results confirm that there are more iron oxides formed on the steel surface in solutions without inhibitor in comparison with solutions containing ZnAlHB HTs. For solutions containing 3ZnAlHB and 4ZnAlHB, the content of Zn is more than that

of 2ZnAlHB. This result indicated the presence of hydrotacite and ZnO formated a thin protective deposited film. The obtained results confirm that the inhibition efficiency of ZnAlHB hydrotalcites depends on Zn/Al ratio. Among the three ZnAlHB hydrotalcites, 3ZnAlHB and 4ZnAlHB provide the better corrosion inhibition for carbon steel in 0.1 M NaCl solution.

4. Conclusions

This work focused to investigate the effect of Zn/Al ratio on the corrosion inhibition of hydrotalcites containing benzoate for carbon steel in NaCl solution. The morphology and structure of ZnAlHB HTs have changes with different Zn/Al ratio. There are no nitrate group and appearance of ZnO in the structure of hydrotalcites with higher Zn/Al ratio (3/1 and 4/1). The surface charge of hydrotalcites decrease

with increase of Zn/Al ratio. In a 0.1 M NaCl solution, the release of benzoate increased with growth of Zn/Al ratio. The inhibition efficiencies of 3ZnAlHB and 4ZnAlHB were higher than that of 2ZnAlHB in 0.1 M NaCl media.

Acknowledgments

References

1. M. Chen, H. Cen, C. Guo, X. Guo, Z. Chen, Preparation of Cu-MOFs and its corrosion inhibition effect for carbon steel in hydrochloric acid solution, *Journal of Molecular Liquids*, **318**, 114328 (2020). Doi: https://doi.org/10.1016/j.molliq.2020.114328

2. A. Fiala, W. Boukhedena, S.E. Lemallem, H. Brahim Ladouani, H. Allal, Inhibition of Carbon Steel Corrosion in HCl and H_2SO_4 Solutions by Ethyl 2-Cyano-2-(1,3-dithian-2-ylidene) Acetate, *Journal of Bio- and Tribo-Corrosion*, **5**, 42 (2019). Doi: https://doi.org/10.1007/s40735-019-0237-5

3. N.A. Negm, N.G. Kandile, E.A. Badr, M.A. Mohammed, Gravimetric and electrochemical evaluation of environmentally friendly nonionic corrosion inhibitors for carbon steel in 1M HCl, *Corrosion Science*, **65**, 94 (2012). Doi: https://doi.org/10.1016/j.corsci.2012.08.002

4. C. Liang, Z. Liu, Q. Liang, G.-C. Han, J. Han, S. Zhang, X.-Z. Feng, Synthesis of 2-aminofluorene bis-Schiff base and corrosion inhibition performance for carbon steel in HCl, *Journal of Molecular Liquids*, **277**, 330 (2019). Doi: https://doi.org/10.1016/j.molliq.2018.12.095

5. A. Thoume, A. Elmakssoudi, D.B. Left, N. Benzbiria, F. Benhiba, M. Dakir, M. Zahouily, A. Zarrouk, M. Azzi, M. Zertoubi, Amino acid structure analog as a corrosion inhibitor of carbon steel in 0.5 M H2SO4: Electrochemical, synergistic effect and theoretical studies, *Chemical Data Collections*, **30**, 100586 (2020). Doi: https://doi.org/10.1016/j.cdc.2020.100586

6. Y. Nie, J. Gao, E. Wang, L. Jiang, L. An, X. Wang, An effective hybrid organic/inorganic inhibitor for alkaline aluminum-air fuel cells, *Electrochimica Acta*, **248**, 478 (2017). Doi: https://doi.org/10.1016/j.electacta.2017.07.108

7. Z. Zheng, O. Olayinka, B. Li, 2S-Soy Protein-Based Biopolymer as a Non-Covalent Surfactant and Its Effects on Electrical Conduction and Dielectric Relaxation of Polymer Nanocomposites, *Engineered Science*, **4**, 87 (2018). Doi: https://dx.doi.org/10.30919/es8d766

8. K. Hu, J. Zhuang, J. Ding, Z. Ma, F. Wang, X. Zeng, Influence of biomacromolecule DNA corrosion inhibitor on carbon steel, *Corrosion Science*, **125**, 67 (2017). Doi: https://doi.org/10.1016/j.corsci.2017.06.004

9. H. Khani, R. Arefinia, Corrosion, Inhibition mechanism of nitrite on the corrosion of carbon steel in simulated cooling water systems, *Materials and Corrosion*, **69**, 337 (2018). Doi: https://doi.org/10.1002/maco.201709735

10. Y. Qiang, S. Zhang, B. Tan, S. Chen, Evaluation of Ginkgo leaf extract as an eco-friendly corrosion inhibitor of X70 steel in HCl solution, *Corrosion Science*, **133**, 6 (2018). Doi: https://doi.org/10.1016/j.corsci.2018.01.008

11. W. Guo, A. Umar, Q. Zhao, M.A. Alsaiari, Y. Al-Hadeethi, L. Wang, M. Pei, Corrosion inhibition of carbon steel by three kinds of expired cephalosporins in 0.1 M H2SO4, *Journal of Molecular Liquids*, **320**, 114295 (2020). Doi: https://doi.org/10.1016/j.molliq.2020.114295

12. A.Y. El-Etre, Physics, Inhibition of C-steel corrosion in acidic solution using the aqueous extract of zallouh root, *Materials Chemistry and Physics*, **108**, 278 (2008). Doi: https://doi.org/10.1016/j.matchemphys.2007.09.037

13. N. El Hamdani, R. Fdil, M. Tourabi, C. Jama, F. Bentiss, Alkaloids extract of Retama monosperma (L.) Boiss. seeds used as novel eco-friendly inhibitor for carbon steel corrosion in 1 M HCl solution: Electrochemical and surface studies, *Applied Surface Science*, **357**, 1294 (2015). Doi: https://doi.org/10.1016/j.apsusc.2015.09.159

14. D. Borisova, D. Akçakayıran, M. Schenderlein, H. Möhwald, D. Shchukin, Nanocontainer?based anticorrosive coatings: effect of the container size on the self?healing performance, *Advanced Functional Materials*, **23**, 3799 (2013). Doi: https://doi.org/10.1002/adfm.201203715

15. W. Li, A. Liu, H. Tian, D. Wang, Controlled Release of Nitrate and Molybdate Intercalated in Zn-Al-Layered Double Hydroxide Nanocontainers towards Marine Anticorrosion Applications, *Colloid and Interface Science Communications*, **24**, 18 (2018). Doi: https://doi.org/10.1016/j.colcom.2018.03.003

16. H. Tian, W. Li, A. Liu, X. Gao, P. Han, R. Ding, C. Yang, D. Wang, Controlled delivery of multi-substituted triazole by metal-organic framework for efficient inhibition of mild steel corrosion in neutral chloride solution, *Corrosion Science*, **131**, 1 (2018). Doi: https://doi.org/10.1016/j.corsci.2017.11.010

17. Z. Zheng, X. Huang, M. Schenderlein, D. Borisova, R.

Cao, H. Möhwald, D. Shchukin, Self‐Healing and Anti-fouling Multifunctional Coatings Based on pH and Sulfide Ion Sensitive Nanocontainers, *Advanced Functional Materials*, **23**, 3307 (2013). Doi: https://doi.org/10.1002/adfm.201203180

18. T.D. Nguyen, A.S. Nguyen, B.A. Tran, K.O. Vu, T.T. Phan, N. Scharnagl, M.L. Zheludkevich, T.X.H. To, Molybdate intercalated hydrotalcite/graphene oxide composite as corrosion inhibitor for carbon steel, *Surface and Coatings Technology*, **399**, 126165 (2020). Doi: https://doi.org/10.1016/j.surfcoat.2020.126165

19. S. K. Poznyak, J. Tedim, L. M. Rodrigues, A. N. Salak, M. L. Zheludkevich, L. F. P. Dick, and M. G. S. Ferreira, Novel inorganic host layered double hydroxides intercalated with guest organic inhibitors for anticorrosion applications, *ACS Applied Materials & Interfaces*, **1**, 2353 (2009). Doi: https://doi.org/10.1021/am900495r

20. E. Alibakhshi, E. Ghasemi, M. Mahdavian, B. Ramezanzadeh, Corrosion inhibitor release from Zn-Al-[PO_4^{3-}]-[CO_3^{2-}] layered double hydroxide nanoparticles, *Progress in Color, Colorants and Coatings*, **9**, 233 (2016).

21. Y. Tang, F. Wu, L. Fang, T. Guan, J. Hu, S. Zhang, A comparative study and optimization of corrosion resistance of ZnAl layered double hydroxides films intercalated with different anions on AZ31 Mg alloys, *Surface and Coatings Technology*, **358**, 594 (2019). Doi: https://doi.org/10.1016/j.surfcoat.2018.11.070

22. R.-C. Zeng, Z.-G. Liu, F. Zhang, S.-Q. Li, H.-Z. Cui, E.-H. Han, Corrosion of molybdate intercalated hydrotalcite coating on AZ31 Mg alloy, *Journal of Materials Chemistry A*, **2**, 13049 (2014). Doi: https://doi.org/10.1039/C4TA01341G

23. X. Yu, J. Wang, M. Zhang, P. Yang, L. Yang, D. Cao, J. Li, One-step synthesis of lamellar molybdate pillared hydrotalcite and its application for AZ31 Mg alloy protection, *Solid State Sciences*, **11**, 376 (2009). Doi: https://doi.org/10.1016/j.solidstatesciences.2008.08.003

24. L. Hou, Y. Li, J. Sun, S.H. Zhang, H. Wei, Y. Wei, Enhancement corrosion resistance of Mg Al layered double hydroxides films by anion-exchange mechanism on magnesium alloys, *Applied Surface Science*, **487**, 101 (2019). Doi: https://doi.org/10.1016/j.apsusc.2019.05.048

25. D. Li, F. Wang, X. Yu, J. Wang, Q. Liu, P. Yang, Y. He, Y. Wang, M. Zhang, Anticorrosion organic coating with layered double hydroxide loaded with corrosion inhibitor of tungstate, *Progress in Organic Coatings*, **71**, 302 (2011). Doi: https://doi.org/10.1016/j.porgcoat.2011.03.023

26. L. Guo, F. Zhang, J.-C. Lu, R.-C. Zeng, S.-Q. Li, L. Song, J.-M. Zeng, A comparison of corrosion inhibition of magnesium aluminum and zinc aluminum vanadate intercalated layered double hydroxides on magnesium alloys, *Frontiers of Materials Science*, **12**, 198 (2018). Doi: https://doi.org/10.1007/s11706-018-0415-2

27. X. Wang, L. Li, Z.-H. Xie, G. Yu, Duplex coating combining layered double hydroxide and 8-quinolinol layers on Mg alloy for corrosion protection, *Electrochimica Acta*, **283**, 1845 (2018). Doi: https://doi.org/10.1016/j.electacta.2018.07.113

28. B. Wu, J. Zuo, B. Dong, F. Xing, C. Luo, Study on the affinity sequence between inhibitor ions and chloride ions in MgAl layer double hydroxides and their effects on corrosion protection for carbon steel, *Applied Clay Science*, **180**, 105181 (2019). Doi: https://doi.org/10.1016/j.clay.2019.105181

29. D.T. Nguyen, H.T.X. To, J. Gervasi, M. Gonon, M.-G. Olivier, Corrosion inhibition of carbon steel by hydrotalcites modified with different organic carboxylic acids for organic coatings, *Progress in Organic Coatings*, **124**, 256 (2018). Doi: https://doi.org/10.1016/j.porgcoat.2017.12.006

30. T.T.X. Hang, T.A. Truc, N.T. Duong, N. Pébère, M.-G. Olivier, Layered double hydroxides as containers of inhibitors in organic coatings for corrosion protection of carbon steel, *Progress in Organic Coatings*, **74**, 343 (2012). Doi: https://doi.org/10.1016/j.porgcoat.2011.10.020

31. T.T.X. Hang, T.A. Truc, N.T. Duong, P.G. Vu, T. Hoang, Preparation and characterization of nanocontainers of corrosion inhibitor based on layered double hydroxides, *Applied Clay Science*, **67**, 18 (2012). Doi: https://doi.org/10.1016/j.clay.2012.07.004

32. T.T.X. Hang, N.T. Duong, T.A. Truc, T. Hoang, D.T.M. Thanh, S. Daopiset, A. Boonplean, Effects of hydrotalcite intercalated with corrosion inhibitor on cathodic disbonding of epoxy coatings, *Journal of Coatings Technology and Research*, **12**, 375 (2015). Doi: https://doi.org/10.1007/s11998-014-9642-3

33. L. Wu, X. Ding, Z. Zheng, Y. Ma, A. Atrens, X. Chen, Z. Xie, D. Sun, F. Pan, Fabrication and characterization of an actively protective Mg-Al LDHs/Al_2O_3 composite coating on magnesium alloy AZ31, *Applied Surface Science*, **487**, 558 (2019). Doi: https://doi.org/10.1016/j.apsusc.2019.05.115

34. Y. Zhao, Y. Chen, W. Wang, Z. Zhou, S. Shi, W. Li, M. Chen, Z. Li, One-step in situ synthesis of nano silver-hydrotalcite coating for enhanced antibacterial and deg-

radation property of magnesium alloys, *Materials Letters*, **265**, 127349 (2020). Doi: https://doi.org/10.1016/j.matlet.2020.127349

35. T.D. Nguyen, A.S. Nguyen, B.A. Tran, K.O. Vu, D.L. Tran, T.T. Phan, N. Scharnagl, M.L. Zheludkevich, T.X.H. To, Molybdate intercalated hydrotalcite/graphene oxide composite as corrosion inhibitor for carbon steel, *Surface and Coatings Technology*, **399**, 126165 (2020). Doi: https://doi.org/10.1016/j.surfcoat.2020.126165

36. T.D. Nguyen, B.A. Tran, K.O. Vu, A.S. Nguyen, A.T. Trinh, G.V. Pham, T.X.H. To, M.V. Phan, T.T. Phan, Corrosion protection of carbon steel using hydrotalcite/graphene oxide nanohybrid, *Journal of Coatings Technology and Research*, **16**, 585 (2018). Doi: https://doi.org/10.1007/s11998-018-0139-3

37. J.E. Olszówka, R. Karcz, E. Bielańska, J. Kryściak-Czerwenka, B.D. Napruszewska, B. Sulikowski, R.P. Socha, A. Gaweł, K. Bahranowski, Z. Olejniczak, E.M. Serwicka, New insight into the preferred valency of interlayer anions in hydrotalcite-like compounds: The effect of Mg/Al ratio, *Applied Clay Science*, **155**, 84 (2018). Doi: https://doi.org/10.1016/j.clay.2018.01.013

38. A.N. Salak, J. Tedim, A.I. Kuznetsova, J.L. Ribeiro, L.G. Vieira, M.L. Zheludkevich, M.G.S. Ferreira, Comparative X-ray diffraction and infrared spectroscopy study of Zn–Al layered double hydroxides: Vanadate vs nitrate, *Chemical Physics*, **397**, 102 (2012). Doi: https://doi.org/10.1016/j.chemphys.2012.01.026

39. Y. Zhang, Y. Li, Y. Ren, H. Wang, F. Chen, Double-doped LDH films on aluminum alloys for active protection, *Materials Letters*, **192**, 33 (2017). Doi: https://doi.org/10.1016/j.matlet.2017.01.038

40. D. Nguyen Thuy, H. To Thi Xuan, A. Nicolay, Y. Paint, M.-G. Olivier, Corrosion protection of carbon steel by solvent free epoxy coating containing hydrotalcites intercalated with different organic corrosion inhibitors, *Progress in Organic Coatings*, **101**, 331 (2016). Doi: https://doi.org/10.1016/j.porgcoat.2016.08.021

41. T.D. Nguyen, A.S. Nguyen, T.T. Thai, G.V Pham, T.X.H. To, M.-G. Olivier, The influence of hydrotalcite intercalated with benzoate on UV stability of acrylic coating, *Corrosion science and Technology*, **19**, 16 (2020), Doi: https://doi.org/10.14773/cst.2020.19.1.16

42. O. Meyer, F. Roessner, R. A. Rakoczy, R. W. Fischer, Impact of Organic Interlayer Anions in Hydrotalcite Precursor on the Catalytic Activity of Hydrotalcite-Derived Mixed Oxides, *Chem.Cat.Chem.*, **2**, 314 (2010). Doi: https://doi.org/10.1002/cctc.200900257

43. A.V. Radha, P. Vishnu Kamath, C. Shivakumara, Mechanism of the anion exchange reactions of the layered double hydroxides (LDHs) of Ca and Mg with Al, *Solid State Sciences*, **7**, 1180 (2005). Doi: https://doi.org/10.1016/j.solidstatesciences.2005.05.004